INTERACTION NOTES

Note 254

1 October 1975

A New Approach Based on a Combination of Integral Equation and Asymptotic Techniques for Solving Electromagnetic Scattering Problems

Raj Mittra and Wai-Lee Ko
Electromagnetics Laboratory
University of Illinois at Urbana-Champaign
Urbana, Illinois

ABSTRACT

In this paper we introduce a new approach for combining the integral equation and high frequency asymptotic techniques, e.g., the geometrical theory of diffraction. The method takes advantage of the fact that the Fourier transform of the unknown surface current distribution is proportional to the scattered far field. A number of asymptotic methods are currently available that provide good approximation to this far field in a convenient analytic form which is useful for deriving an initial estimate of the Fourier transform of the current distribution. An iterative scheme is developed for systematically improving the initial form of the high frequency asymptotic solution by manipulating the integral equation in the Fourier transform domain. A salient feature of the method is that it provides a convenient validity check of the solution for the surface current distribution by verifying that the surface of the scatterer. Another important feature of the method is that it yields both the induced surface current density and the far field. Diffraction by a strip (two-dimensional problem) and diffraction by a thin plate (three-dimensional problem) are presented as illustrative examples that demonstrate the usefulness of the approach for handling a variety of electromagnetic scattering problems in the resonance region and above. Some concluding remarks and comparison with other methods are also included.

ACKNOWLEDGEMENT

The work reported in this paper was supported in part by the U. S. Army Research Office under Grant DAHC04-74-G-0113 and in part by the Office of Naval Research Grant N00014-75-C-0293. The authors are pleased to acknowledge many helpful comments and criticisms of their colleagues at the Electromagnetics Laboratory of the University of Illinois, especially to Professor G. A. Deschamps, Professor S. W. Lee and Dr. Y. Rahmat-Samii.

I. INTRODUCTION

It is well-known that the integral equation methods are limited in application to scatterers whose characteristic dimensions are of the order of one wavelength or less. On the other hand, the high-frequency asymptotic techniques can be reliably used only when the scatterer is large compared to the wavelength, and neither of the above two methods is suitable in the resonance region. This paper introduces a new hybrid technique*, based on a combination of the integral equation and asymptotic methods, that is useful in the entire frequency range encompassing the resonance region and above. Another important feature of the method is that it can be used to check and improve the accuracy of high-frequency asymptotic solutions. Such an accuracy test and systematic improvement of the asymptotic solution are often needed, but no reliable methods for performing these are available at the present time.

In contrast to the ray optics methods, which are based on the diffraction of ray fields as determined by the local properties of the surface of the scatterer, the present method starts with the integral equation formulation incorporating the boundary conditions on the entire surface of the scatterer. Conventionally, the solution of the integral equation for the induced surface current is carried out by matrix methods [9], [10]. The size of the matrix becomes prohibitively large and its solution extremely time-consuming when the characteristic dimension of the scatterer approaches the wavelength of the illuminating field. The approach developed in this paper circumvents this difficulty while still preserving the self-consistent nature of the integral equation formulation by constructing the solution in the Fourier transform or spectral domain rather than in the space domain. We take advantage of the facts that the Fourier transform of the surface

*The original concepts on which this paper is based were described at the 1975 URSI Symposium in a paper entitled "A New Method for Improving the GTD Solution Via the Integral Equation Formulation," by R. Mittra and W. L. Ko.

current distribution *is* directly proportional to the far scattered field and that the asymptotic methods often provide a very good initial estimate of the latter quantity. We next construct an iterative* solution of the integral equation in the transform domain with the GTD or other high-frequency solution as the zero-order approximation. As shown in the paper, this procedure not only allows us to improve on the GTD or similar solutions but also provides a convenient means for testing the satisfaction of the boundary conditions on the surface of the scatterer. Furthermore, the method yields not only the far-field but also the induced surface-current distribution, a feature not readily available in some other high frequency techniques.

The application of the general procedure outlined above is illustrated by two examples: the two-dimensional problem of a plane wave diffraction by a strip and a three-dimensional problem of a plane wave diffraction by a thin plate. These problems were chosen for the following reasons. It is shown that when the angle of incidence is normal or near normal, the GTD solution accurately satisfies the boundary condition $\bar{E}_{tan} = 0$ on the strip even when the multiple interaction between the two edges of the strip is neglected. However, it is found that when the angle of incidence is near grazing, the GTD solution is quite unsatisfactory, while the iterated solution generated by the hybrid technique does display the correct behavior. In the plate problem, the difficulty in applying GTD to this geometry stems from the fact that the diffraction coefficient for the corners of the plate is not known and neglecting the corner effects can cause substantial errors in the resonance frequency region where the plate

---

*A moment method solution in the spectral domain has also been developed. See Ref. [3].

size is of the order of one wavelength squared. The case of the solid surface scatterer is not included in this paper but will be the subject of a forthcoming publication.

Before closing this section, we mention two other innovative hybrid techniques [1], [2] that have recently been reported in the literature. We will briefly compare these methods with the one described in this paper in Section VI, and point out the similarities and the differences.

II. FORMULATION

We begin our analysis with the electric-field integral equation [11] for a perfectly conducting scatterer. The equation may be symbolically written as

$$(\bar{\bar{G}} * \bar{J})_t = -\bar{E}^i_t \quad , \quad \bar{r}\varepsilon S \tag{1}$$

where $\bar{J}(\bar{r}')$ is the induced surface current density we are attempting to determine, and the subscript t signifies tangential to the surface S; $\bar{E}^i_t$ is the tangential component of the incident electric field $\bar{E}^i$ on the surface S of the scatterer; and $\bar{\bar{G}}$ is the Green's Dyadic, which yields the scattered electric field when operating on $\bar{J}$. In anticipation of Fourier transforming (1), we extend it over all space by first defining a truncation operator θ as follows:

For any vector $\bar{A}(\bar{r})$, which is a vector function of position $\bar{r}$

$$\theta(\bar{A}) = \bar{A}_t \, \delta(\bar{r} - \bar{r}_s) \quad , \quad \bar{r}_s \varepsilon S$$

where $\delta(\bar{r} - \bar{r}_s)$ is the Dirac delta function and the subscript t signifies tangential to the surface S. Also its complementary operator $\hat{\theta}$ is defined as

$$\hat{\theta}(\bar{A}) = \bar{A} - \theta(\bar{A}) \quad .$$

We can then rewrite (1) as

$$\bar{\bar{G}} * \bar{J} = \theta(-\bar{E}^{i}) + \hat{\theta}(\bar{\bar{G}} * (\theta\bar{J})) \quad , \text{ for all space.} \tag{2}$$

As indicated above, (2) is valid at all observation points whether on or off the surface S. Note that the integral equation (1) is embedded in (2) and that we have made use of the obvious identity $\theta\bar{J} = \bar{J}$.

Next we Fourier transform (2) by introducing the transform relationships

$$\tilde{F}(\bar{k}) = \int_{-\infty}^{\infty} F(\bar{r})\ e^{-i\bar{k}\cdot\bar{r}}\ d\bar{r} = \mathcal{F}[F(\bar{r})] \tag{3a}$$

and

$$F(\bar{r}) = (\frac{1}{2\pi})^3 \int_{-\infty}^{\infty} \tilde{F}(\bar{k})\ e^{i\bar{k}\cdot\bar{r}}\ d\bar{k} = \mathcal{F}^{-1}[\tilde{F}(\bar{k})] \tag{3b}$$

with $\sim$ on top denoting the transformed quantities.

The transformed version of (2) reads

$$\tilde{\bar{\bar{G}}}\tilde{\bar{J}} = -\tilde{\bar{E}}_I + \tilde{\bar{F}} \tag{4}$$

where $\tilde{\bar{F}} = \mathcal{F}[\hat{\theta}(\bar{\bar{G}} * (\theta J))]$, and $\tilde{\bar{E}}_I$ is the transform of the tangential component of the incident field truncated on S. Note that the convolution operation in (2) is transformed into an algebraic product upon Fourier Transformation.

A formal solution to (4) can now be written

$$\tilde{\bar{J}} = \tilde{\bar{\bar{G}}}^{-1}(-\tilde{\bar{E}}_I + \tilde{\bar{F}}) \quad . \tag{5}$$

Equation (5) says that if we had available the Fourier transform of the scattered electric field, we could construct the solution for the induced surface current density in the transform domain by adding it to $-\tilde{\bar{E}}_I$, which is known, and by performing an algebraic division represented by $\tilde{\bar{\bar{G}}}^{-1}$. In practice, of course, $\tilde{\bar{F}}$ is not known and must be solved for along with $\tilde{\bar{J}}$ if (5) is to be used in the form as shown. However, instead of using this form, we proceed to derive an iterated form of the equation as shown below:

$$\tilde{\bar{J}}^{(n+1)} = \tilde{\bar{G}}^{-1}(-\tilde{\bar{E}}_I + \tilde{\bar{F}}^{(n)}) \tag{6}$$

which indicates the (n + 1)th approximation of $\tilde{\bar{J}}$ from the nth approximation for $\tilde{\bar{F}}$. We next show how $\tilde{\bar{F}}^{(n)}$ itself can be derived from $\tilde{\bar{J}}^{(n)}$. To this end, we use the identity

$$\tilde{\bar{F}} = F[F^{-1}[\tilde{\bar{G}}\tilde{\bar{J}}] - \theta(F^{-1}[\tilde{\bar{G}}\tilde{\bar{J}}])] \tag{7}$$

which may be verified by writing (7) as

$$\tilde{\bar{F}} = F[\bar{\bar{G}} * \bar{J} - \theta(-\bar{E}^i)] \tag{8}$$

and using (2) to get

$$\tilde{\bar{F}} = F[\hat{\theta}(\bar{\bar{G}} * (\theta\bar{J}))] \tag{9}$$

which, of course, is the definition of $\tilde{\bar{F}}$. We can now use (7) to derive the nth approximation $\tilde{\bar{F}}^{(n)}$ of $\tilde{\bar{F}}$ from the nth approximation of $\bar{J}$, i.e., $\bar{J}^{(n)}$. The relationship is written as

$$\tilde{\bar{F}}^{(n)} = F[F^{-1}[\tilde{\bar{G}}\tilde{\bar{J}}^{(n)}] - \theta(F^{-1}[\tilde{\bar{G}}\tilde{\bar{J}}^{(n)}])] \quad . \tag{10}$$

The desired iteration relating $\tilde{\bar{J}}^{(n+1)}$ and $\tilde{\bar{J}}^{(n)}$ may now be written. Using (6) and (10)

$$\tilde{\bar{J}}^{(n+1)} = \tilde{\bar{G}}^{-1}[-\tilde{\bar{E}}_I + F[F^{-1}[\tilde{\bar{G}}\tilde{\bar{J}}^{(n)}] - \theta(F^{-1}[\tilde{\bar{G}}\tilde{\bar{J}}^{(n)}])]] \tag{11}$$

The step-by-step procedure for constructing the solution of the transformed surface current $\bar{J}$ will now be given:

1. Begin with an estimate of $\tilde{\bar{J}}^{(0)}$, which is the Fourier transform of the induced surface current, or equivalently, the scattered *far field* within a known multiplicative constant. Typically, $\tilde{\bar{J}}^{(0)}$ is available from GTD or other asymptotic solutions for the diffracted field in an analytic form and hence the transform $\tilde{\bar{J}}^{(0)}$ is known over both the visible and the invisible ranges.

2. Multiply $\tilde{\bar{J}}^{(0)}$ by $\tilde{\bar{\bar{G}}}$, the known transform of the Green's Dyadic. Note this involves algebraic multiplication and not the usual time-consuming convolution operation.

3. Take the inverse Fourier transform of the product $\tilde{\bar{\bar{G}}}\tilde{\bar{J}}^{(0)}$ using both *visible and invisible ranges.*

4. Apply the truncation operator θ to $F^{-1}[\tilde{\bar{\bar{G}}}\tilde{\bar{J}}^{(0)}]$, which gives the approximation to the tangential component of the scattered electric field $\bar{E}_t^s$ on the surface S. The accuracy of the solution can be conveniently checked at this point by verifying the satisfaction of the boundary condition by the tangential component of $\bar{E}^s$, viz., $\{\bar{E}_t^s = -\bar{E}_t^i\}$ on S. As mentioned in Section I, this is an important feature of the method.

5. Subtract $\theta(F^{-1}[\tilde{\bar{\bar{G}}}\tilde{\bar{J}}^{(0)}])$ from the total $F^{-1}[\tilde{\bar{\bar{G}}}\tilde{\bar{J}}^{(0)}]$ already evaluated.

6. Take the Fourier transform of the difference obtained in Step 5.

7. Subtract $\tilde{\bar{E}}_I$, the Fourier transform of the tangential component of the incident electric field truncated on the surface, from the result in Step 6.

8. Multiply the result obtained in Step 7 by $\tilde{\bar{\bar{G}}}^{-1}$. Note that $\tilde{\bar{\bar{G}}}^{-1}$ is also known and the operation is again algebraic as in Step 2. The result thus obtained is $\tilde{\bar{J}}^{(1)}$, which is the first iteration of the scattered far field.

9. Take the inverse Fourier transform of $\tilde{\bar{J}}^{(1)}$ obtained in Step 8 and evaluate it on S to get the desired induced surface current on the scatterer. In other words, perform the operation $\theta(F^{-1}[\tilde{\bar{J}}^{(1)}])$. For an exact solution, this operation is redundant, since $\bar{J} = \theta\bar{J}$, and hence, $\theta(F^{-1}[F[\theta\bar{J}]]) = \theta\theta\bar{J} = \bar{J}$. However, the Fourier inversion of an nth approximate solution $\tilde{\bar{J}}^{(n)}$ will not give rise to a current distribution that is nonzero except on S.

This step provides a test for the accuracy and for the convergence of the approximate solution by comparing the approximate $\tilde{\tilde{J}}^{(0)}$ with $F[\Theta(F^{-1}[\tilde{\tilde{J}}^{(1)}])]$.

10. Take $F[\Theta(F^{-1}[\tilde{\tilde{J}}^{(1)}])]$ to derive an *improved* approximation for $\tilde{\tilde{J}}^{(1)}$.

11. Repeat as necessary using, for instance, the *improved* $\tilde{\tilde{J}}^{(1)}$ from Step 10 in the iteration Equation (11) to generate the next higher-order approximation $\tilde{\tilde{J}}^{(2)}$.

In the following two sections, we show, in some detail, the application of the procedure just described to a two-dimensional and a three-dimensional scattering problem.

III. DIFFRACTION BY AN INFINITE STRIP

The geometry of the electromagnetic scattering problem involving a perfectly conducting infinite strip of zero thickness illuminated by a uniform plane wave, whose electric intensity vector is oriented parallel to the edges of the strip, is depicted in Figure 1. For convenience of analysis, an arbitrary incident wave can always be decomposed into two components with respect to the z-axis, namely, TM_z (E-wave) and TE_z (H-wave). In the following discussion we consider the E-wave case only; the H-wave case can be solved in a similar manner by considering $\overline{H}^i = \hat{z}\, H_o^i$.

The incident field is given by

$$E_z^i(\rho,\phi) = e^{-ik(x\cos\phi_o + y\sin\phi_o)} \quad , \tag{12}$$

where the $e^{-i\omega t}$ time dependence is understood. The integral equation formulation [5] for the problem at hand takes the form

$$-E_z^i(x) = \int_{-a}^{a} J_z(x')\, G(x - x')\, dx', \quad x\in[-a,a] \quad , \tag{13}$$

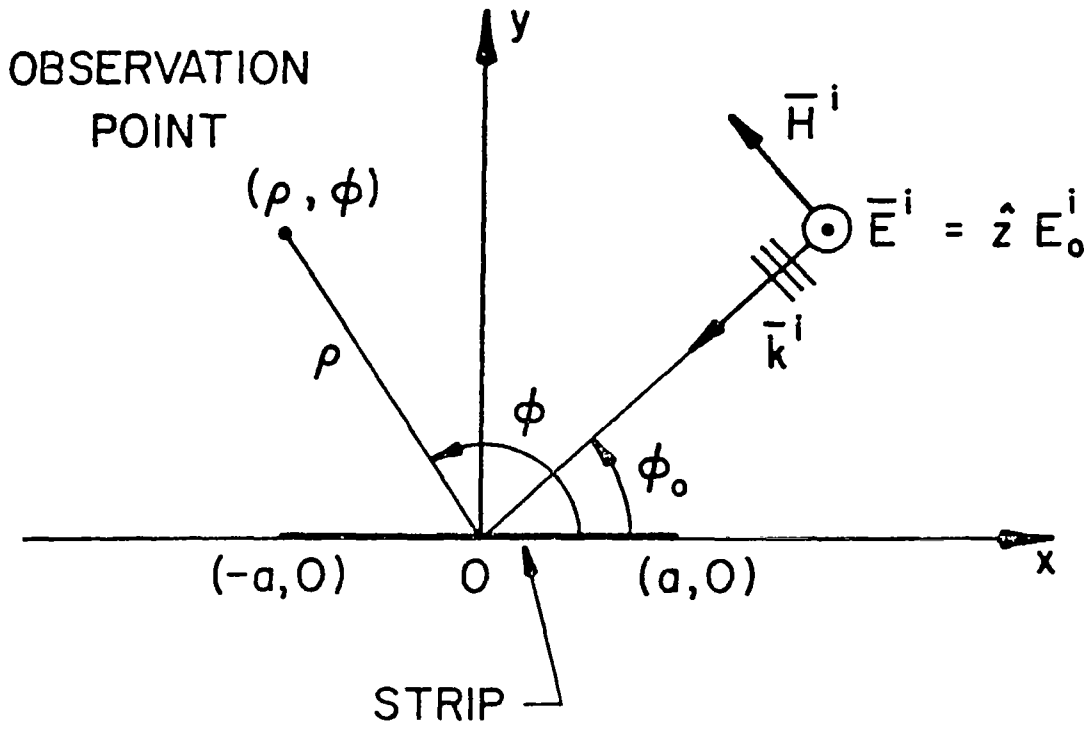

Figure 1. Diffraction by a strip illuminated by an E-wave.

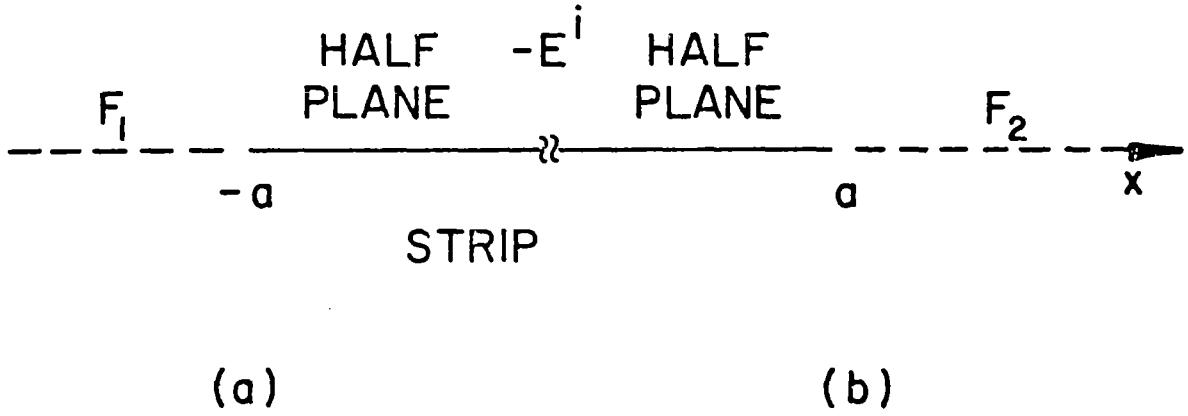

Figure 2. $F_1(x)$ can be approximated by the GTD solution to the half-plane problem (a) shown on the left-hand side; $F_2(x)$ can be approximated by the GTD solution to the half-plane problem (b) shown on the right-hand side.

where $J_z(x')$ is the algebraic sum of the induced surface current densities on the top and the bottom surfaces of the thin strip. The kernel G is the two-dimensional free-space Green's function given by

$$G(x - x') = \frac{i}{4} H_o^{(1)}(k_o|x - x'|) \quad , \tag{14}$$

where $H_o^{(1)}$ is the Hankel's function of the first kind of order zero. $k_o = 2\pi/\lambda$ is the free-space propagation constant. Note that (13) is the conventional integral equation which equates the integral representation of the tangential component of the scattered E-field radiated by the induced surface current density to the negative of the tangential component of the incident E-field on the surface of the perfectly conducting scatterer as required by the satisfaction of the boundary condition. Hence (13) is valid on the strip only. An extended integral equation that is valid for all x can be obtained by including the scattered fields outside the strip as well. If the scattered field on the interval $(-\infty,-a)$ is designated by $F_1(x)$ and the scattered field on the interval (a,∞) is designated by $F_2(x)$, then the extended form of (13) becomes

$$\int_{-a}^{a} J_z(x')\, G(x - x')\, dx' = \theta(-E_z^i(x)) + F_1(x) + F_2(x) \quad , \tag{15}$$

where θ is defined in Section II. Since the Fourier transform of the induced surface current density can be related to the far field, (15) is Fourier-transformed to give

$$\tilde{J}_z(\alpha)\, \tilde{G}(\alpha) = \widetilde{\theta(-E_z^i)}\ (\alpha) + \tilde{F}_1(\alpha) + \tilde{F}_2(\alpha) \quad , \tag{16}$$

where ~ on top indicates the Fourier transform pair defined in (3) which simplifies in the present one-dimensional problem to

$$\tilde{F}(\alpha) = \int_{-\infty}^{\infty} F(x)\, e^{-i\alpha x}\, dx \tag{17a}$$

and

$$F(x) = \frac{1}{2\pi} \int_{-\infty}^{\infty} \tilde{F}(\alpha)\, e^{i\alpha x}\, d\alpha \quad . \tag{17b}$$

The Fourier transform of the two-dimensional Green's function in (16) takes the form

$$\tilde{G}(\alpha) = \frac{i}{2\sqrt{k_o^2 - \alpha^2}} \quad . \tag{18}$$

Note that (16) is an algebraic equation in the spectral domain in contrast to the convolution form of the integral equation (15) in the spatial domain. The reason for working in the spectral domain will become clear when the method of solution for (16) is developed. Following the procedure discussed in Section II and in terms of the notations introduced in the present problem, we proceed as follows:

1. Obtain $\tilde{J}_z^{(0)}(\alpha)$, the zero-order approximation of the Fourier transform of the induced surface current density from GTD or any other asymptotic expression for the far-field, including <u>both</u> the visible and invisible ranges.

2. Derive $\hat{0}\left(\tilde{J}_z^{(0)}(\alpha)\,\tilde{G}(\alpha)\right)$ to approximate $\tilde{F}_1^{(0)}(\alpha) + \tilde{F}_2^{(0)}(\alpha)$. Note that GTD may be used to get closed-form expressions for $\tilde{F}_1^{(0)}(\alpha)$ and $\tilde{F}_2^{(0)}(\alpha)$ since $F_1(x)$ and $F_2(x)$ can be approximated by the GTD solutions to the two half-plane problems as shown in Figure 2.

3. Solve for $\tilde{J}_z^{(1)}(\alpha) = F\,0\left\{F^{-1}\left[\dfrac{0(-E^i)(\alpha) + \tilde{F}_1^{(0)}(\alpha) + \tilde{F}_2^{(0)}(\alpha)}{\tilde{G}(\alpha)}\right]\right\}$.

4. Repeat as necessary.

The check for satisfaction of the integral equation can be applied very simply by computing $\tilde{J}(\alpha)\,\tilde{G}(\alpha)$, taking its inverse Fourier transform, and verifying how well it approaches $-E_i$ on the surface of the scatterer. Galerkin's method applied in the spectral domain can also be employed to systematically improve the solution by using, for instance, $\tilde{J}^{(0)}(\alpha)$, $\tilde{J}^{(1)}(\alpha)$, etc., as the basis.

Figure 3 shows the calculated induced surface current density distribution on the strip with ka = 4 (1.3λ wide) for normal incidence. Note that the current density becomes large at the edges, as it should for E-wave incidence, although no specific condition was enforced at the edges, nor any special care exercised. Note also that the approximate current is confined essentially on the surface of the strip and extends very little outside of this surface. Thus, the solution in this case is very close to the true solution and this is easily verified by truncating the current density, computing the scattered field it radiates on the strip, and verifying that the scattered field is indeed very nearly equal to $-E_i$. Figure 4 shows the result for ka = 40 i.e., a 13λ strip. Note that the peak in the center is no longer present and the current there approaches that given by the physical optics approximation. There are now more oscillations, however, and the current density has a sharp dip before rising to infinity at the edges. Figure 5 shows the moment method applied in the spectral domain solution [6] and the comparison with the one obtained here is quite favorable. Figure 6 shows the satisfaction of the boundary condition after one iteration. As mentioned before, such a test is not available in the conventional GTD approach.

Let us next turn to the interesting case of a near grazing incidence where the zero-order current density has a long tail extending beyond the edge of the strip (see Figure 7). This result is to be expected since the two half-plane GTD solutions used in the zero-order approximation represent a poor approximation for the induced current for shallow incidence angles. If this tail is truncated, the remaining portion of the current density on the strip produces a scattered field on the surface of the strip which is significantly different from $-E^i$, as may be seen from Figure 8. Figure 9 shows the effect of one iteration on the zero-order GTD solution

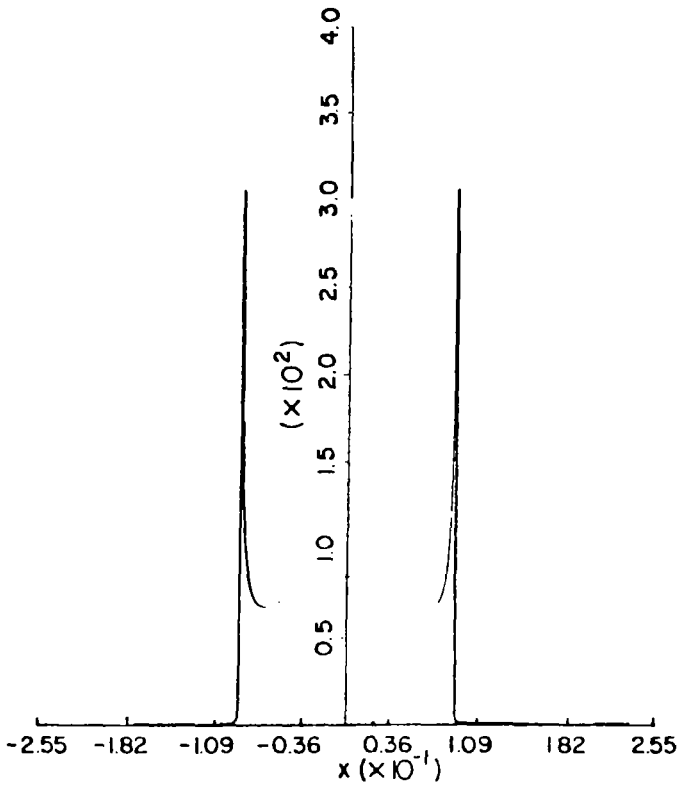

Figure 3. Magnitude of the induced surface current density distribution normalized to $(ik_o Z_o)^{-1}$ on the strip of $ka \cong 4$. (1.273 λ wide), $\phi_o = 90^\circ$.

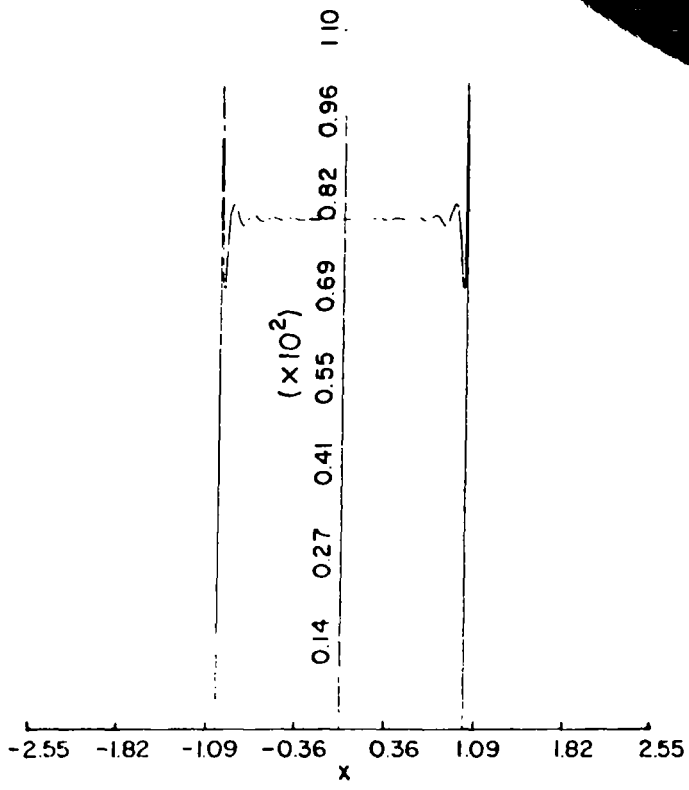

Figure 4. Magnitude of the induced surface current density distribution normalized to $(ik_o Z_o)^{-1}$ on the strip of $ka \cong 40$. (12.73 λ wide), $\phi_o = 90^\circ$.

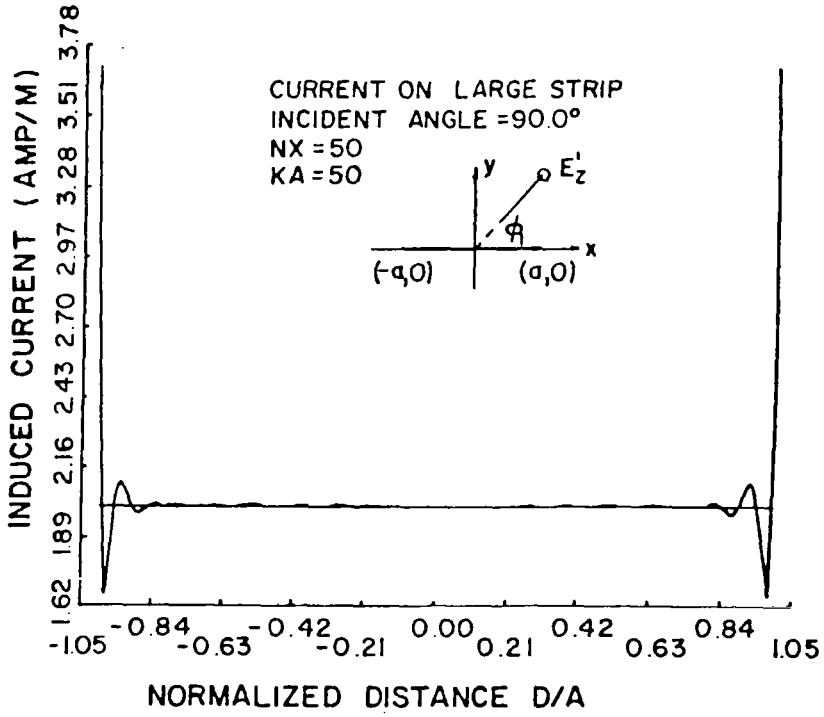

Figure 5. Moment method (applied in the spectral domain) solution of the magnitude of the induced surface current density distribution normalized to $1/Z_o$ on the strip of ka = 50. (15.92 λ wide), $\phi_i = 90^\circ$.

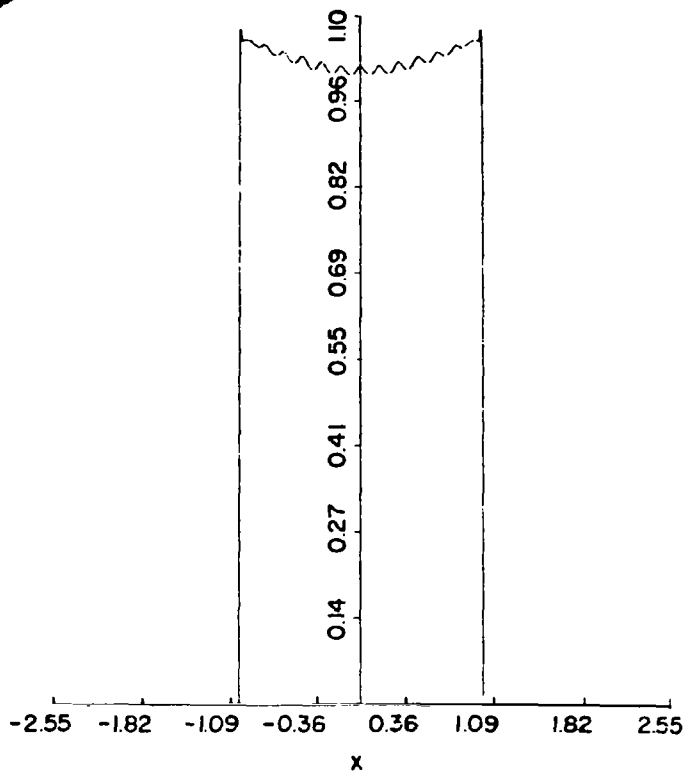

Figure 6. Magnitude of the scattered E-field evaluated on the strip of ka = 40., $\phi_o = 90^o$ (one iteration).

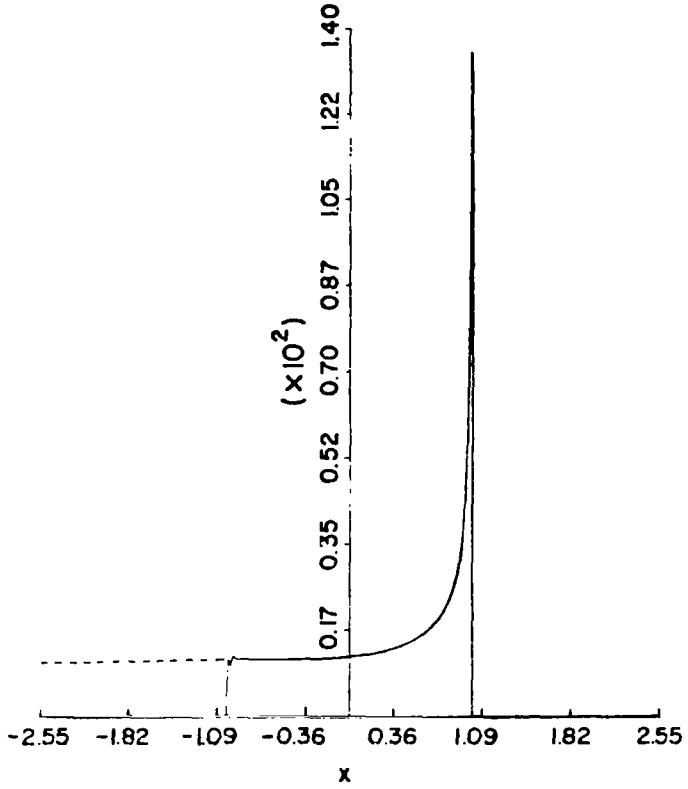

Figure 7. Magnitude of the induced surface current density distribution normalized to $(ik_o Z_o)^{-1}$ on the strip of ka = 40., $\phi_o = 10^o$ (no iteration).

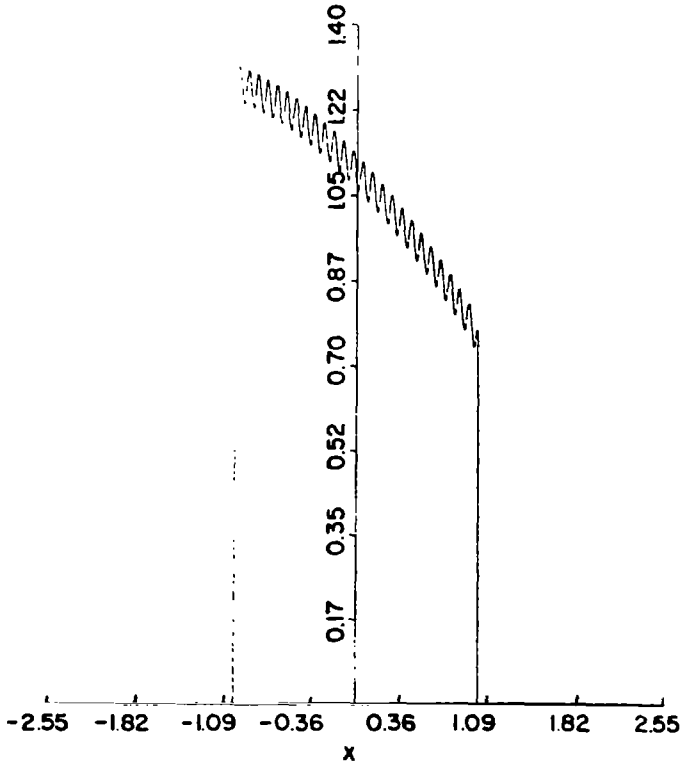

Figure 8. Magnitude of the scattered E-field evaluated on the strip of ka = 40., $\phi_o = 10^o$ (no iteration).

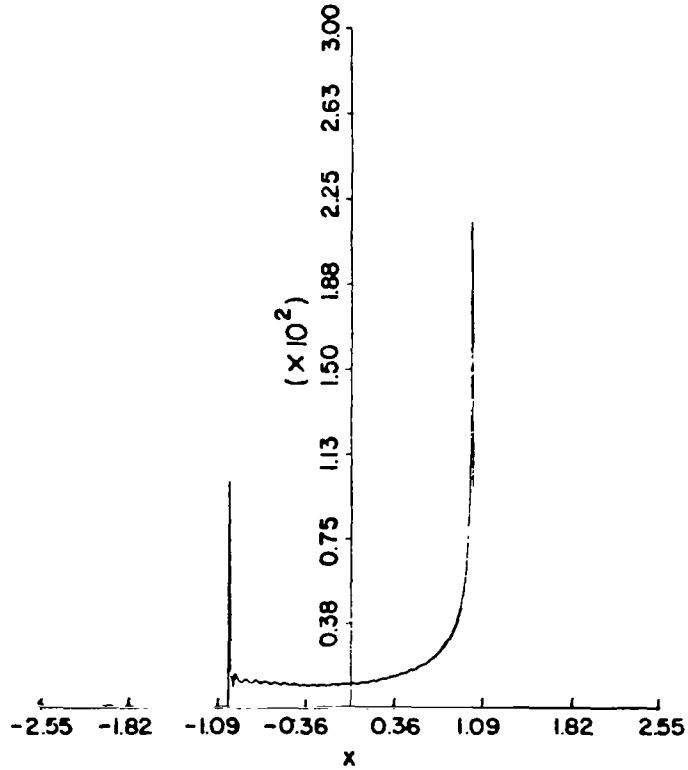

Figure 9. Magnitude of the induced surface current density distribution normalized to $(ik_o Z_o)^{-1}$ on the strip of ka = 40., $\phi_o = 10^o$ (one iteration).

shown in Figure 7. Note that the current density is significantly altered in the neighborhood of the shadowed edge. To see that this is indeed an improved solution, the truncated portion of it is used to calculate the scattered field. It is observed that the satisfaction of the boundary condition has been improved as shown in Figure 10. To verify the convergence of the solution numerically, one more iteration is performed and the result is depicted in Figure 11. Note that the shape of the surface current density does not change much which indicates a settling down of the solution has occurred. Also, note that the tail extending outside of the strip has been reduced to an insignificant quantity, which, when truncated, will produce little effect on the scattered field on the surface of the strip. To further validate the solution, the moment method solution [6] of the same problem with slightly different parameters is shown in Figure 12 for a comparison. Again, the agreement is good.

Before closing this section, it is worthwhile to recapitulate the main points of the approach discussed. The strip problem has been solved by a combination of the integral equation and asymptotic high frequency techniques. Formulation of the integral equation in the Fourier transform domain allows one to conveniently obtain the zero-order approximation to the transformed unknown surface current density from the solution of two half-plane problems. Higher-order solutions have been obtained via the iteration steps outlined above and the numerical convergence has been demonstrated. Validity of the solution has been substantiated by numerically verifying the satisfaction of the boundary condition.

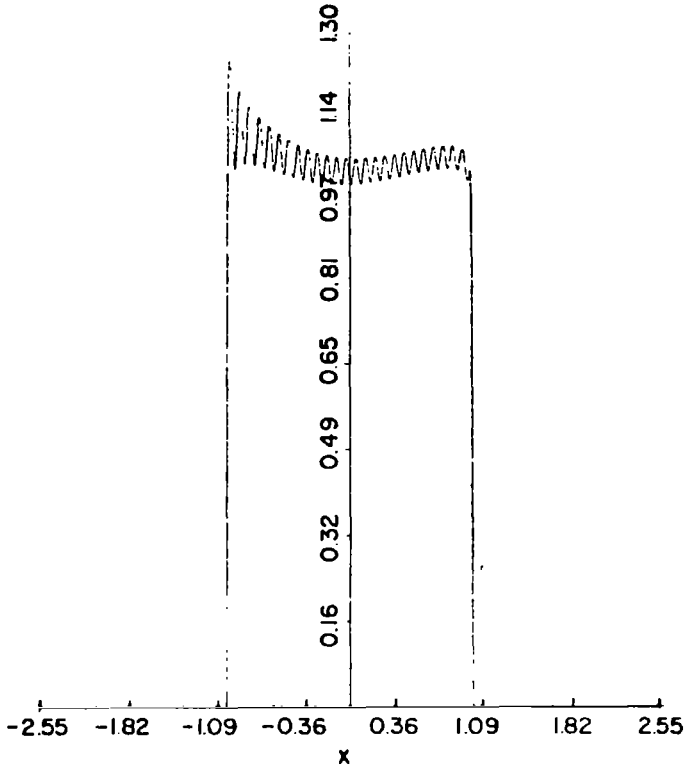

Figure 10. Magnitude of the scattered E-field evaluated on the strip of ka = 40., ϕ_o = 10° (one iteration).

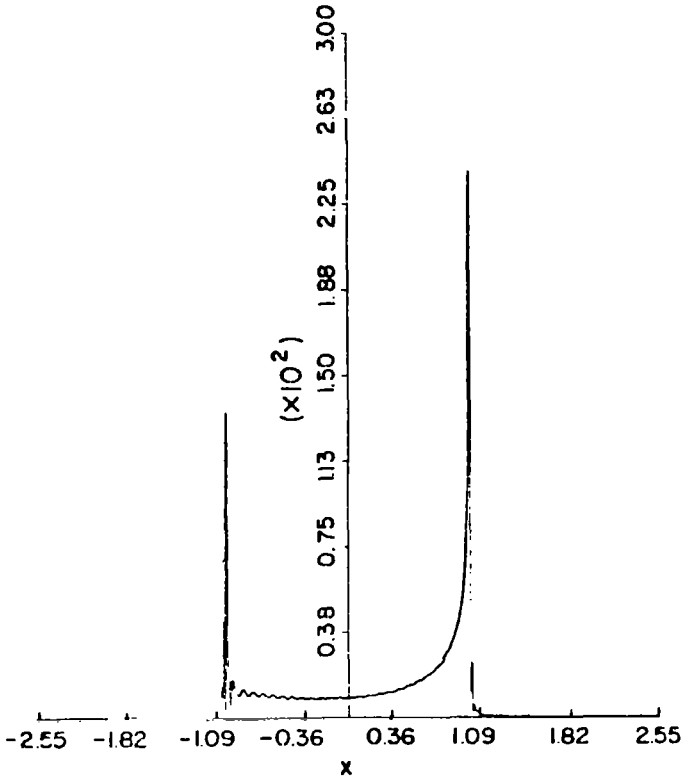

Figure 11. Magnitude of the induced surface current density distribution normalized to $(ik_o Z_o)^{-1}$ on the strip of ka = 40., ϕ_o = 10° (two iterations).

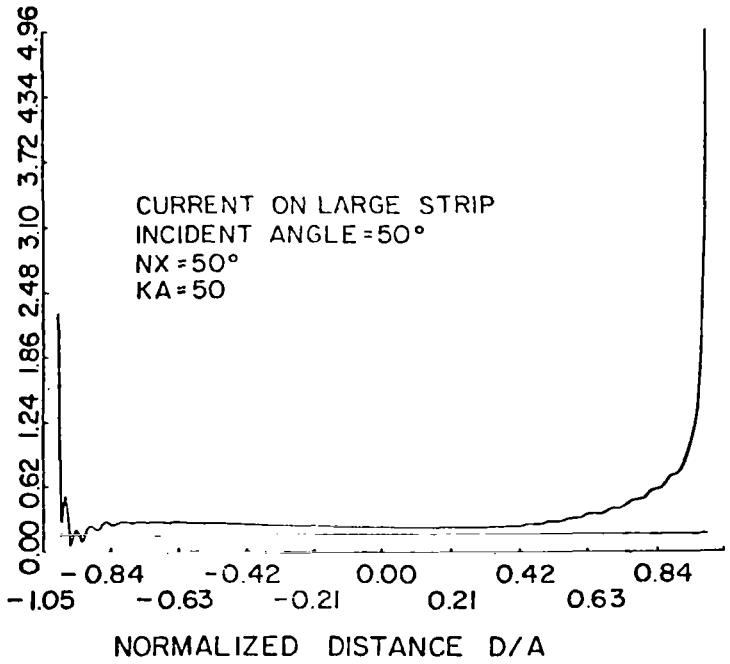

Figure 12. Moment method (applied in the spectral domain) solution of the magnitude of the induced surface current density distribution normalized to $1/Z_o$ on the strip of ka = 50., ϕ_o = 5°.

IV. DIFFRACTION BY A FINITE THIN PLATE

Having illustrated the usefulness of the hybrid technique for combining the integral equation and GTD techniques relevant to a two-dimensional scatterer, viz., the strip, we now turn to the more general three-dimensional problem, a thin rectangular plate illuminated by a plane wave. For the sake of simplicity we consider only the case of an $\hat{x}$-polarized uniform plane wave which is normally incident on a square thin plate. The geometry of the problem is depicted in Figure 13, where the plate is located in the $z = 0$ plane. Using classical electromagnetic theory, the following coupled integro-differential equations are readily obtained:

$$\left(\frac{\partial^2}{\partial x^2} + k^2\right) A_x(x,y) + \frac{\partial^2}{\partial x \partial y} A_y(x,y) = i\omega\mu_0 E_x^i(x,y) \tag{19a}$$

and

$$\left(\frac{\partial^2}{\partial y^2} + k^2\right) A_y(x,y) + \frac{\partial^2}{\partial x \partial y} A_x(x,y) = 0 \tag{19b}$$

where $x\varepsilon(-a,a)$, $y\varepsilon(-b,b)$, and $z = 0$. A_x and A_y in (19a) and (19b) are the x- and the y-components of the magnetic vector potential, respectively. Since the convolution of the induced surface current density with the free-space Green's function gives the magnetic vector potential, we have the expressions which are valid in the $z = 0$ plane

$$A_x(x,y) = J_x(x,y) * G(x - x', y - y') \quad , \tag{20a}$$

and

$$A_y(x,y) = J_y(x,y) * G(x - x', y - y') \quad , \tag{20b}$$

where * denotes the convolution operation and the free-space Green's function is given by

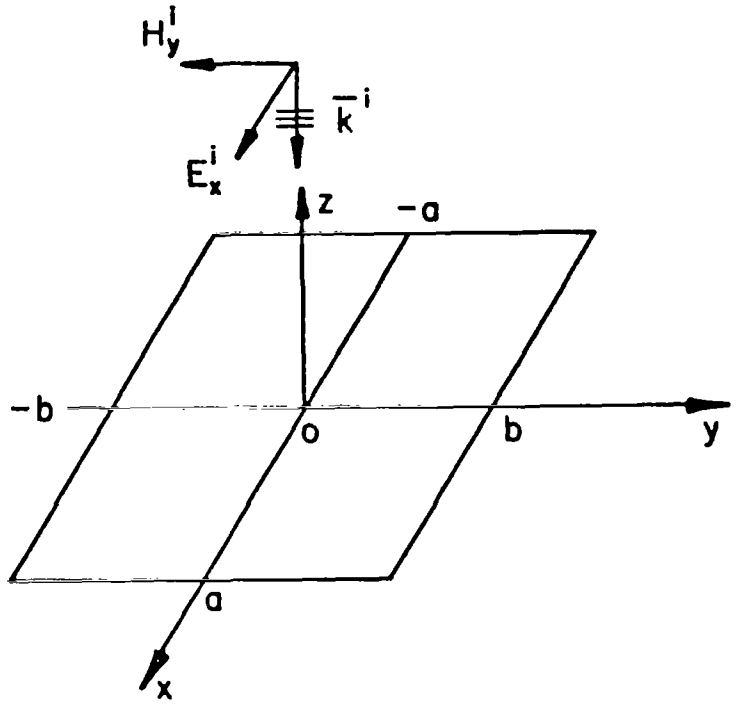

Figure 13. Diffraction by a finite rectangular thin plate illuminated by a normally incident plane wave with polarization as shown.

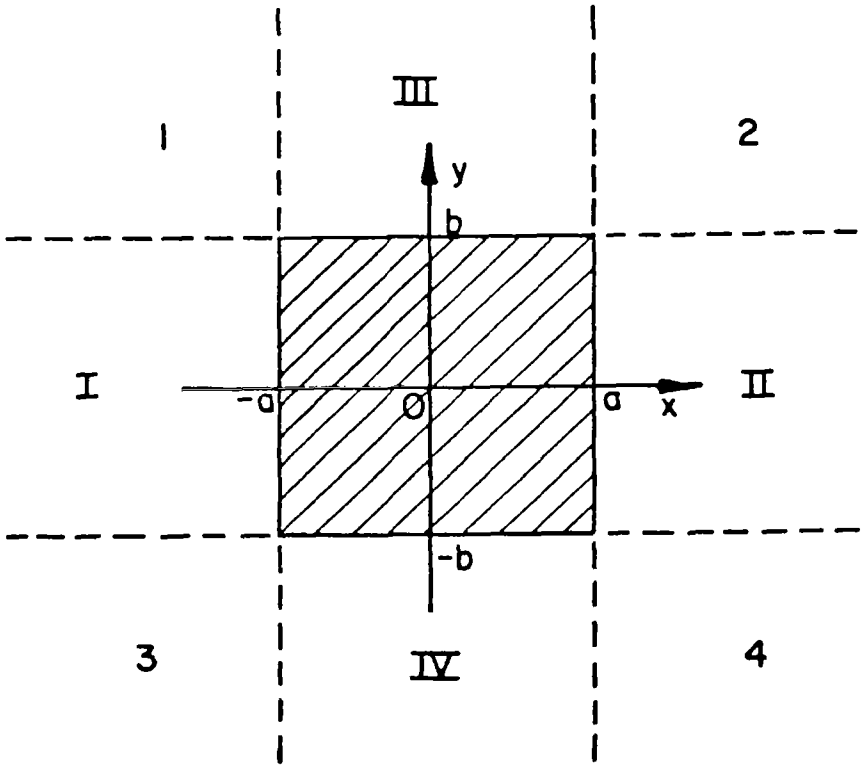

Figure 14. Regions in the z = 0 plane in each of which the zero-order approximation of the scattered field is obtained according to Table 1.

$$G(x - x', y - y') = \frac{1}{4\pi} \frac{\exp(ikr)}{r} \tag{21}$$

where

$$r = \sqrt{(x - x')^2 + (y - y')^2}, \quad z, z' = 0 \quad .$$

Note that (19a) (19b) are conventional integro-differential equations which are valid on the plate only. To obtain an extended form of these equations, additional unknown functions $F_x(x,y)$ and $F_y(x,y)$ will be introduced. The domain of these functions is the region complementary to the plate in the $z = 0$ plane. Hence, the extended form of (19a) (19b) can be written as

$$\left(\frac{\partial^2}{\partial x^2} + k^2\right) A_y(x,y) + \frac{\partial^2}{\partial x\, \partial y} A_y(x,y) = -i\omega\varepsilon_o \left[-\theta\left\{E_x^i(x,y)\right\} + \hat{\theta}\left\{F_x(x,y)\right\}\right], \tag{22a}$$

and

$$\left(\frac{\partial^2}{\partial y^2} + k^2\right) A_y(x,y) + \frac{\partial^2}{\partial x\, \partial y} A_x(x,y) = -i\omega\varepsilon_o \hat{\theta} F_y(x,y) \quad , \tag{22b}$$

where θ and $\hat{\theta}$ are operators defined in Section II. Note that (22a) (22b) are valid for the entire $z = 0$ plane. These equations are now Fourier transformed to obtain

$$(\alpha^2 - k^2) \tilde{J}_x(\alpha,\beta) \tilde{G}(\alpha,\beta) + \alpha\beta \tilde{J}_y(\alpha,\beta) \tilde{G}(\alpha,\beta) = \frac{ik_o}{Z_o}\left[\widetilde{-\theta(E_x^i)}(\alpha,\beta) + \widetilde{\hat{\theta}(F_x)}(\alpha,\beta)\right] \tag{23a}$$

and

$$(\beta^2 - k^2) \tilde{J}_y(\alpha,\beta) \tilde{G}(\alpha,\beta) + \alpha\beta \tilde{J}_x(\alpha,\beta) \tilde{G}(\alpha,\beta) = \frac{ik_o}{Z_o} \widetilde{\hat{\theta}(F_y)}(\alpha,\beta) \quad , \tag{23b}$$

where $\sim$ on top indicates the Fourier transform as defined in (17a) with transform variables (α,β) corresponding to (x,y), respectively, and $Z_o = \sqrt{\mu_o/\varepsilon_o}$ is the free-space impedance. In writing (23a) and (23b), (20a) and (20b) have been utilized. The Fourier transform of the free-space Green's function, specialized to the $z = 0$ plane as given in (21), is

$$\tilde{G}(\alpha,\beta) = \frac{i}{2}\frac{1}{\sqrt{k_o^2 - \alpha^2 - \beta^2}} \quad . \tag{24}$$

Observe that (23a), (23b) are two algebraic equations in the transform domain as opposed to the two integro-differential equations in (22a) and (22b). It is a simple step to derive the zero-order solutions of $\tilde{J}_x(\alpha,\beta)$ and $\tilde{J}_y(\alpha,\beta)$ once the estimates of $\widetilde{\hat{\theta}(F_x)}(\alpha,\beta)$ and $\widetilde{\hat{\theta}(F_y)}(\alpha,\beta)$ are available. One merely solves the two coupled algebraic equations for these two unknowns $\tilde{J}_x(\alpha,\beta)$ and $\tilde{J}_y(\alpha,\beta)$. For the present case, $\hat{\theta}(F_y)(x,y)$ is zero due to the particular choice of $\hat{x}$-polarized normal incident plane-wave illumination. With this in mind, the first-order solutions of the transformed surface current density can be expressed as

$$\tilde{J}_x(\alpha,\beta) = \frac{2}{\sqrt{k_o^2 - \alpha^2 - \beta^2}}\left[\frac{\beta^2 - k_o^2}{k_o Z_o}\right]\left[-\widetilde{\theta(E_x^i)}(\alpha,\beta) + \widetilde{\hat{\theta}(F_x)}(\alpha,\beta)\right], \tag{25a}$$

and

$$\tilde{J}_y(\alpha,\beta) = \frac{-2}{\sqrt{k_o^2 - \alpha^2 - \beta^2}}\left[\frac{\alpha\beta}{k_o Z_o}\right]\left[-\widetilde{\theta(E_x^i)}(\alpha,\beta) + \widetilde{\hat{\theta}(F_x)}(\alpha,\beta)\right]. \tag{25b}$$

$\tilde{J}_x(\alpha,\beta)$ and $\tilde{J}_y(\alpha,\beta)$ are then inverse Fourier-transformed and truncated to obtain the induced surface current densities on the plate.

Next, we estimate the zero-order approximation to $\hat{\theta}(F_x)(x,y)$ using the GTD solutions to four pertinent half-plane problems. The $z = 0$ plane containing the plate has been divided into regions as shown in Figure 14, where the hatched region is occupied by the plate and the scattered field in this region must be equal to the $-\theta(E^i(x,y))$ to satisfy the boundary condition. The rest of the $z = 0$ plane has been designated by digital numbers and Roman numerals, and the manner in which the scattered fields in these various regions are obtained is concisely tabulated in Table 1.

TABLE 1

THE ZERO-ORDER APPROXIMATION OF $\hat{\theta}(F_x(x,y))$ IN VARIOUS REGIONS EXTERNAL TO THE PLATE OBTAINED VIA THE USE OF GTD METHOD

REGION	SCATTERED FIELD	REMARKS
I, II	$E_x(x,z = 0)$	DERIVED FROM H-WAVE STRIP GTD SOLUTION
III, IV	$E_x(y,z = 0)$	DERIVED FROM E-WAVE STRIP GTD SOLUTION
1, 2, 3, 4	0	FIRST ESTIMATE

In deriving the zero-order approximation, the *scattered* fields in regions 1, 2, 3 and 4 are neglected although these fields are nonzero in higher-order approximations. The zero-order approximation to the scattered fields is computed in regions III and IV, by starting with the E-wave GTD solution for the strip, and truncating it so that it is nonzero only in these regions. In regions I and II, the H-wave GTD solution for a strip is used to obtain $H_y(x,z = 0)$, and then $E_x(x,z = 0)$ is constructed from Maxwell's equations. The resulting solution is again truncated so that it is nonzero only in the appropriate regions.

Having completed the estimation of the zero-order approximation to the scattered field $\hat{\theta}(F_x(x,y))$ external to the plate, we now proceed to solve for the induced surface current on the plate. To this end we return to (25a) and (25b) and substitute the Fourier transform of $\hat{\theta}(F_x(x,y))$ and compute $\tilde{J}_x$ and $\tilde{J}_y$. The desired induced surface current densities in the space domain are then obtained by inverse Fourier transformation and truncation. If necessary, the iteration scheme discussed in the previous sections can be

followed to obtain higher-order solutions. Convergence of the solution can be checked by performing one more iteration and checking to see whether the solution has "settled down." Validity of the solution can be assured by computing the scattered field on the plate using the solution of the surface current just obtained to see how well the boundary condition is satisfied on the surface of the plate. It should be clear now that all of these steps follow exactly the same line as in the case of the strip problem discussed in Section III.

The numerical result for the dominant x-component of the surface current density for a one-wavelength squared plate is shown in Figure 15a. Note that the surface current density, which goes to zero at the two edges perpendicular to the incident electric intensity vector, tends to grow without bound at the other two edges parallel to the incident electric intensity vector, although no special edge condition has been enforced to derive this behavior. To see that edge behavior better, a 90° rotation of the surface current in Figure 15a is shown in Figure 15b. It is clearly seen from Figure 15b that the cross section of the x-component of the surface current density at $x = 0$ closely resembles the surface current on the strip plotted in Figure 3. Figures 16a, 16b, and 16c exhibit the change in the behavior of the current distribution both in the middle of the plate and at the corners as the plate size is progressively increased. Figures 17a and 17b show the cross-polarized component of the surface current density on the plate. This current density goes to zero at the line of symmetry in the middle of the plate and has a tendency to grow without bound at the edges. The results for the one-wavelength squared plate have been checked by moment method solutions and the agreement is good. For such an electrically small plate, results are available for

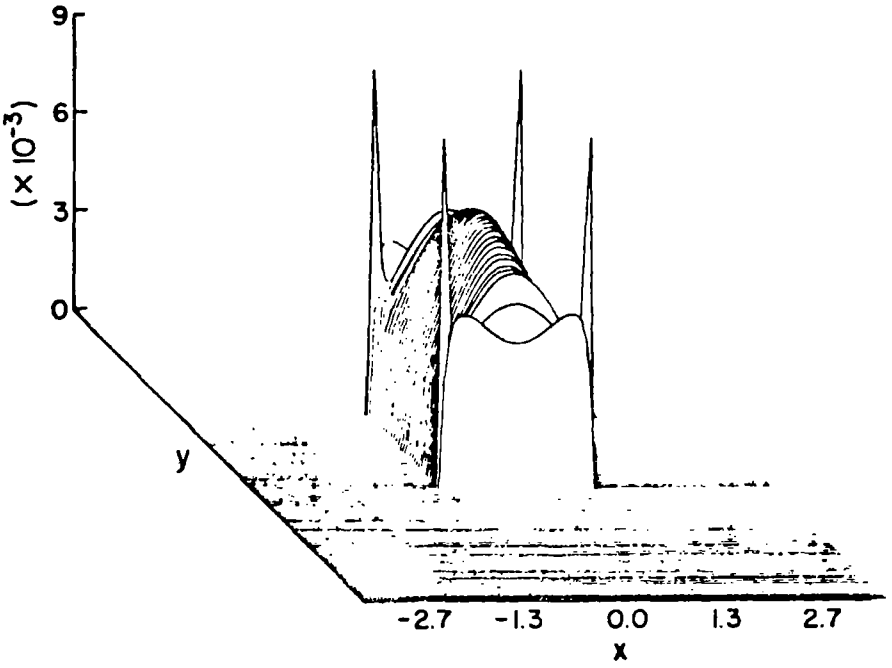

Figure 15a. Magnitude of the dominant x-component of the surface current density on a 1λ x 1λ plate (ka = 3.14) with normal incidence; plate region: xε(-1,1), yε(-1,1).

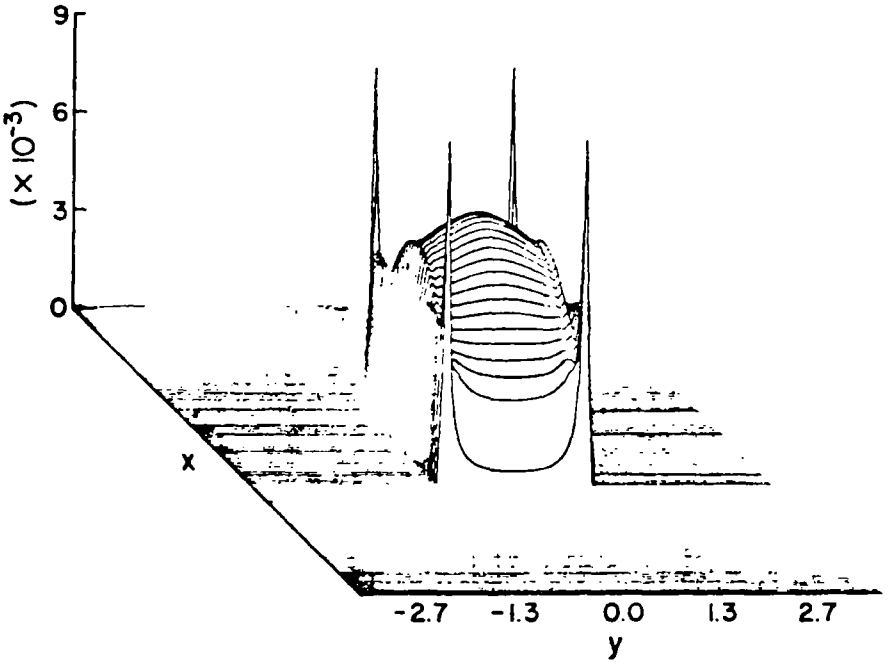

Figure 15b. A 90° rotation of the surface current in Figure 15a.

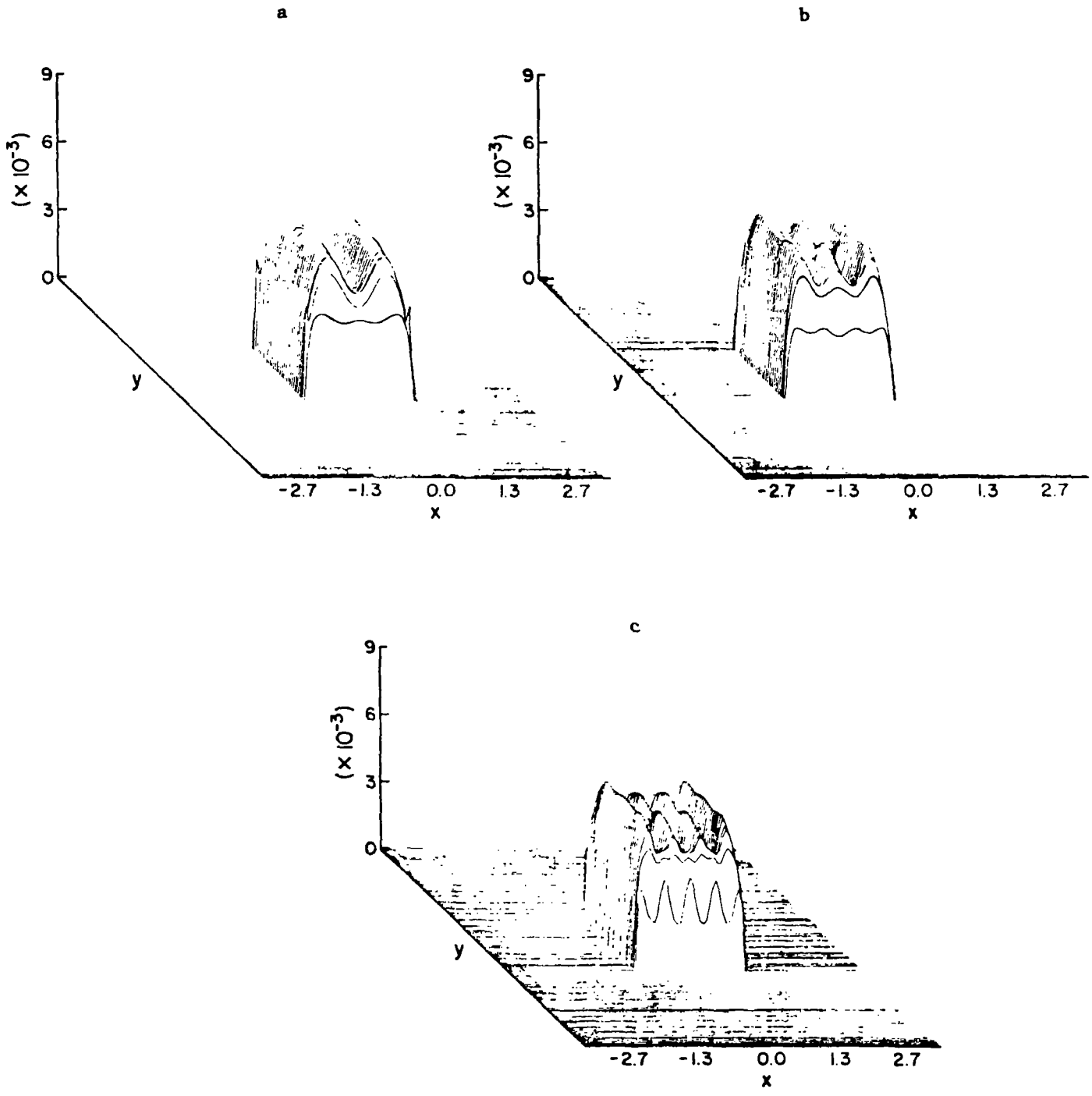

Figure 16. Magnitudes of the dominant x-components of the surface current density on: (a) a $2\lambda \times 2\lambda$ plate ($ka = 6.28$), (b) a $3\lambda \times 3\lambda$ plate ($ka = 9.43$), and (c) a $4\lambda \times 4\lambda$ plate ($ka = 12.6$); plate region: $x\varepsilon(-1,1)$, $y\varepsilon(-1,1)$, normal incidence with x-polarization.

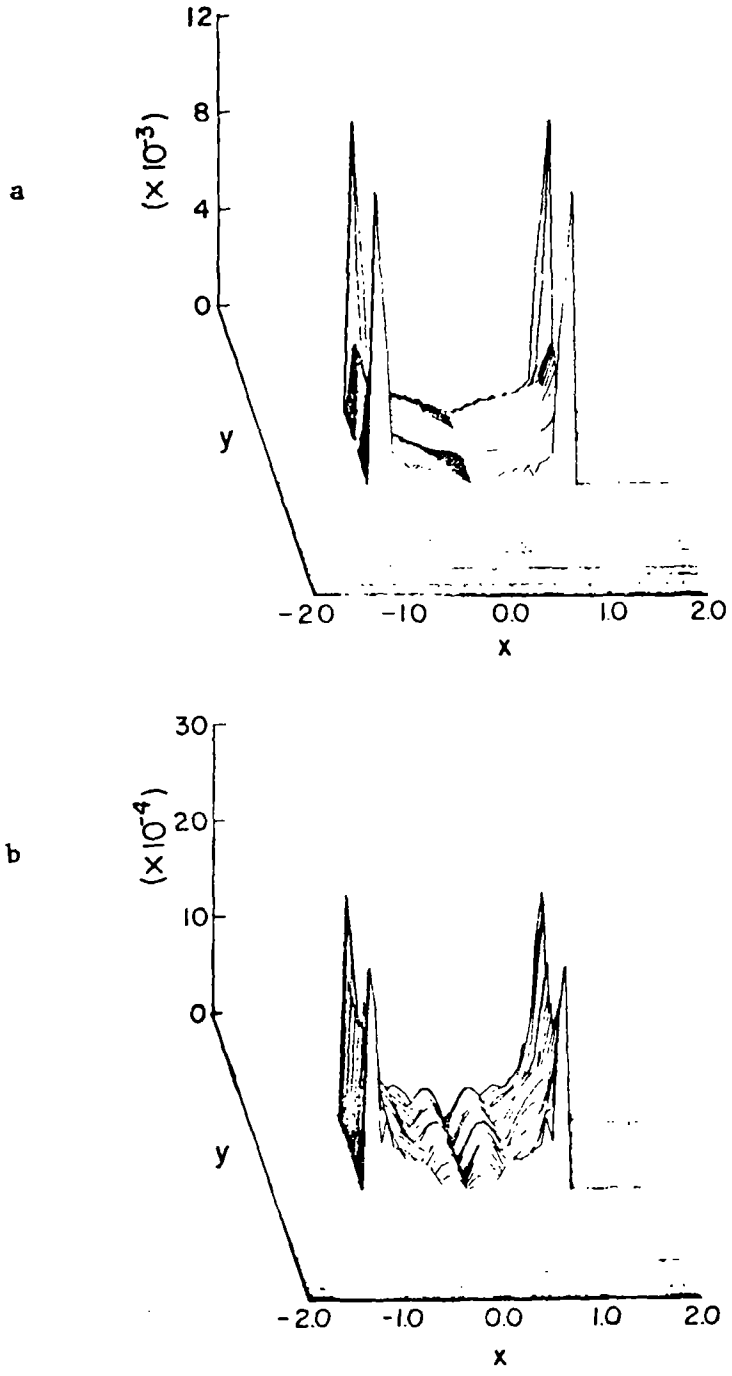

Figure 17. Magnitudes of the cross-polarized components of the surface current density on: (a) a 1λ x 1λ plate (ka = 3.14), and (b) a 3λ x 3λ plate (ka = 9.43); plate region: xε(-1,1), yε(-1,1), normal incidence with x-polarization.

comparison in the literature [6], [7]. However, for electrically large plates the matrix size becomes prohibitively large when the conventional moment method type of approach is used. In contrast, the accuracy and the convergence of the solution improve even further for a large scatterer. It should also be mentioned that the number of grid points at which the current density of the plate has been evaluated is 2048. Such fine details of the current behavior would also be impractical to obtain using the moment method.

V. COMPUTATIONAL CONSIDERATIONS

An important step in the method of solution outlined in the previous sections of the present approach is the computation of the Fourier and the inverse Fourier transforms from the spatial to the spectral domains and vice versa. To perform the Fourier transformation using the digital computer, both the spatial and the spectral functions are discretized into sets of samples, i.e., a Discrete Fourier Transform (DFT) is employed. The well-known Cooley-Tukey Fast Fourier Transform (FFT) [8] allows one to compute the DFT with only $N \log_2 N$ operations for N data samples, thus, reducing the computational time to a few seconds even for a large N. It must be realized, however, that the FFT algorithm generates a periodic representation of the true Fourier transform. Care should be exercised to assure that the aliasing error is small by sampling the function to be transformed often enough to comply with the Nyquist sampling rate. Furthermore, the Gibbs' phenomenon due to the finiteness of the sampling window should be suppressed by using one of the window functions known in the field of digital signal processing. To this end, a simple, but highly effective Hamming window can be conveniently incorporated into the computer program as a minimal requirement for a digital low-pass filter.

It is worth mentioning that in the strip problem discussed in Section II, all of the numerical results including the computer plots are generated within a few seconds on the IBM360/75 computer. Even for the plate problem discussed in Section III, the computational time involved is only of the order of one minute. This demonstrates the fact that the method of computation is numerically very efficient.

VI. CONCLUDING REMARKS

A new approach for combining the integral equation and high frequency asymptotic techniques has been demonstrated with two illustrative examples--diffraction by a strip (two-dimensional problem) and a thin plate (three-dimensional problem). The basic idea is to start with the asymptotic high frequency solution leading to the zero-order approximation of the scattered far field, and to use the latter in the Fourier-transformed version of the extended form of the integral equation to derive an improved result for the induced surface current density. By formulating the problem in the spectral domain, the spatial domain integral equation becomes an algebraic equation, which can be recast in an iteration scheme suitable for manipulations on the computer. A salient feature of the method is that the accuracy of the solution for the surface current density can be conveniently checked by verifying whether the scattered field, which is also computed in the process of generating the solution, indeed satisfies the boundary condition at the surface of the scatterer. Therefore, this approach not only provides a way for systematically improving the GTD solution using the self-consistent, integral equation formulation, but also provides a convenient validity check of the ray optics solution. Furthermore, the method of solution yields both the induced surface current density and the far field--an important feature which is not present in conventional asymptotic high frequency methods.

The convergence of the iterative scheme has not been proven rigorously but has been demonstrated by numerical verification only. It should be pointed out, however, that Galerkin's scheme in the spectral domain can always be employed in place of the iteration procedure if a need for the use of the Galerkin's method is clearly justified. Although only scattering objects with infinitesimal thickness have been investigated in this paper, the method itself is general enough to handle a much larger class of geometries, including bodies with finite thickness. The investigation of such structures is currently in progress and will be reported in a future publication.

Finally, we would like to mention two other approaches [1], [2] that are based on a combination of asymptotic and integral equation techniques. The one developed by Thiele [1] decomposes a given problem into two parts, one of which is handled using the GTD method and the other using the moment method. For the case of a wire antenna on a finite ground plane, the effect of the edge diffraction from the ground plane is evaluated using GTD and the result is subsequently used to augment the impedance matrix of the monopole antenna over an infinite ground plane. Although the method works rather well when GTD results are accurately known for the ground plane problem, e.g., a ground plane of circular shape, no convenient method is available for improving the solution when there are corners in the plane that contribute substantially to the scattered field. The latter situation arises when the ground plane is of rectangular shape and is not large compared to the wavelength, or when the antenna is mounted close to one or more of the edges.

The second method developed by Burnside [2] tends to rectify the situation alluded to above by solving for surface currents via the moment

method in the regions where the GTD solution is not accurate, and by using asymptotic forms for the surface currents in regions where a good approximation for these currents can be employed. However, this method cannot be conveniently applied to either the strip problem with grazing incidence, or to the large plate problem discussed in this paper. For the strip problem, the GTD solution is quite inaccurate when the incident angle of the illuminating wave is near grazing. For the plate problem, the current does not settle down to known asymptotic form in the center region of the plate until it is at least three to four wavelengths squared. The moment method is incapable of handling the number of unknowns required to accurately solve for the current distribution on plate sizes that are larger than 2λ squared.

One other method developed by Bojarski [12] should be mentioned for completeness since he also uses the transform technique to convert the integral equation into an algebraic form. However, he uses a three-dimensional Fourier transform which again becomes unwieldly, both in terms of computer storage and time. In contrast, the present method employs two-dimensional transforms even for a three-dimensional structure, thus achieving a saving in the storage requirement by approximately two orders of magnitude and a corresponding saving in CPU and I/O times as well. Although, to date, we have investigated only three-dimensional problems with geometries that have planar faces or angular symmetries, the possibility of generalizing the approach to more general shapes appears to be quite promising. One other point with respect to Bojarski's work is that no advantageous use is made of the available analytic form of the GTD solution for the far field in the visible and invisible ranges, which, in many cases, forms an excellent starting point of the iteration procedure.

REFERENCES

[1] G. A. Thiele and T. H. Newhouse, "A hybrid technique for combining moment methods with the geometrical theory of diffraction," IEEE Trans. on Antennas and Propagation, vol. AP-23, pp. 62-69, January 1975.

[2] W. D. Burnside, C. L. Yu and R. J. Marhefka, "A technique to combine the geometrical theory of diffraction and the moment method," IEEE Trans. on Antennas and Propagation, vol. AP-23, pp. 551-558, July 1975.

[3] R. Mittra and T. S. Li, "A spectral domain approach to the numerical solution of electromagnetic scattering problems," AEÜ, vol. 29, pp. 217-222, 1975.

[4] R. Mittra and S. W. Lee, Eds., Analytical Techniques in the Theory of Guided Waves. Macmillan, New York, p. 81, 1971.

[5] A. W. Maue, "Formulation of general diffraction problems through an integral equation," Zeltschrift fur Physik, vol. 126, pp. 601-618, 1949.

[6] Y. Rahmat-Samii and R. Mittra, "Integral Equation Solution and RCS Computation of a Thin Rectangular Plate," Interaction Note 156, December 1973.

[7] J. L. Lin, W. L. Curtis and M. C. Vincent, "On the field distribution of an aperture," IEEE Trans. on Antennas and Propagation, vol. AP-22, pp. 467-471, May 1974.

[8] IEEE Trans. on Audio and Electroacoustics, June 1967, a special issue on the FFT.

[9] R. F. Harrington, Field Computation by Moment Methods, Macmillan, New York, 1968.

[10] R. Mittra, Ed., Computer Techniques for Electromagnetics, Pergamon Press, Oxford, 1973.

[11] A. J. Poggio and E. K. Miller, "Integral Equation Solutions for Three Dimensional Scattering Problems," in Ref. [10], Chapter 4, 1973.

[12] N. N. Bojarski, "K-space formulation of the electromagnetic scattering problem," Technical Report AFAL-TR-71-75, March 1971.